Composites Science and Technology 137 (2016) 118–129

Contents lists available at ScienceDirect

Composites Science and Technology

journal homepage: http://www.elsevier.com/locate/compscitech

Preparation and electrorheological behavior of anisotropic titanium oxide/polyaniline core/shell nanocomposite

Xiaoli Tian [a, b], Kai He [a, b], Chengwei Wang [a, b], Qingkun Wen [a, b], Baoxiang Wang [a, b, *], Shoushan Yu [a, b], Chuncheng Hao [a, b], Kezheng Chen [a, **], Qingquan Lei [a, b]

[a] College of Materials Science and Engineering, Qingdao University of Science and Technology, Qingdao 266042, PR China
[b] State Key Laboratory of Electrical Insulation and Power Equipment, Xi'an Jiaotong University, Xi'an 710049, PR China

ARTICLE INFO

Article history:
Received 30 July 2016
Received in revised form
27 October 2016
Accepted 28 October 2016
Available online 1 November 2016

Keywords:
Smart materials
Nano composites
Mechanical properties
Electrorheological fluid

ABSTRACT

Anisotropic titanium oxide/polyaniline core/shell nanocomposite was synthesized via a three-step method, and its electrorheological (ER) properties under external applied electric field were researched. Firstly, monodispersed amorphous titanium oxide nanospheres were prepared by a controlled hydrolysis method and then anisotropic titanium oxide peanut-like nanospheres was obtained by using weak acid to etch the monodispersed titanium oxide sphere. At last, the surface of anisotropic TiO_2 was coated with polyaniline (PANI) through an *in-situ* polymerization method. Then the influence factors on the preparation of anisotropic TiO_2/polyaniline core/shell structure nanoparticles were discussed deeply, including different kinds and amounts of acid, the amount of aniline, and so on. The morphology and structure of the samples were characterized by scanning electron microscopy, transmission electron microscopy, zeta potential analysis and X-ray powder diffraction, respectively. The electrorheological behaviors of the anisotropic TiO_2/polyaniline composite particles are characterized using a rotational rheometer, which shown a good ER activity.

1. Introduction

The electrorheological (ER) fluid is a kind of intelligent materials whose rheological characters can be changed reversibly according to the external applied electric field [1–14]. An electrorheological system mostly composed of solid particles, and insulating carrier medium. The solid particles can be metallic oxide, inorganic, organic, and organic/inorganic composites [15–19]. For a variety of materials which used for ER solid particles, the electrical conductivity is a key parameter that needs to be satisfied with the semiconducting. In order to meet the conditions, researchers prepared many composites. The reason for that is because the electrical conductivity of composites is much more controllable than single material. Generally, the whole ER system is colloids, suspensions, and emulsions. Because of this nature of the ER fluid, make it has the application in varied control equipments, such as dampers and actuators controlled. But, ER system have several limitations such as easily electrical breakdown at high electrical field, low stability, and low shear strength, which largely restrict it's industry application [20–24]. To overcome these limitations, various types of materials have been introduced as ER dispersed materials. For instance, polymer/inorganic composite were used because of their high polarization ability attributed to the difference in chemical and physical structure.

At present, Titanium dioxide (TiO_2) has been becomes one of the most extensively researched semiconducting materials. Titanium oxide has many peculiar properties such as a wide band gap of 3.2 eV, low cost, chemical stability, etc. [25]. It also can be used in many fields, especially in photo catalysis, lithium-ion batteries, and solar energy [26]. As we all known, there is a great relationship between material performance and its morphology and structure. So, many people have done many words to synthesis novel structures of TiO_2. Recently, the research focuses on the one-dimensional nanotube and nanowire, two-dimensional nanosheets, hierarchical structures, hollow or porous structure, etc. [27–29] Among the conducting polymers, polyaniline (PANI) have a good prospect because it possess a lot of advantages, such as cheap raw materials, simple synthesis processes, controllable conductivity, good environmental stability and process ability. At present,

* Corresponding author. College of Materials Science and Engineering, Qingdao University of Science and Technology, Qingdao 266042, PR China.
** Corresponding author.
E-mail addresses: bxwang@qust.edu.cn (B. Wang), kchen@qust.edu.cn (K. Chen).

http://dx.doi.org/10.1016/j.compscitech.2016.10.026
0266-3538/

soft or hard templates were used to achieve PANI nanostructure. The combination of high dielectric TiO_2 and good conductive PANI with complex structure may provide high ER activity and application.

In addition, core-shell particles are an interesting design for ER materials, especially for better ER performance. Considering the dielectric TiO_2 and conducting polymers, the dielectric effects of core particles can be combined with the electrical properties of conducting shell layers. Therefore, anisotropic structured particles may provide high dielectric response, which is beneficial to the enhancement of ER activity. So, in this work, we prepared a kind composite that is made up of conducting polymers-PANI and semiconducting inorganic oxide-TiO_2, which also combine the advantage of core-shell and anisotropic structure. The prepared anisotropic TiO_2/polyaniline core/shell particles were dispersed in silicone oil and their electro-responsive ER properties were tested at various electric field strengths.

2. Experimental section

2.1. Synthesis of the monodispersed titanium oxide nanospheres

Monodispersed titanium oxide spherical particles were prepared by controlled hydrolysis of tetrabutyl titanate (TBT, $[CH_3(CH_2)_3O]_4Ti$, 98% purity) in ethanol. Firstly, 0.5 mL of 0.1 M aqueous potassium chloride was added into 100 mL ethanol, and then stirred 30 min. Secondly, 2 mL of TBT was added to above solution at ambient temperature. The solution was stirred strongly using a magnetic stirrer for about 10 min until a white precipitate appeared. Thirdly, the suspension was aged in a static condition for 24 h in a closed container at room temperature. The powder deposited at the bottom of the vessel was collected and washed it with ethanol and de-ionic water for several times, then dried at 50 °C in air.

2.2. Synthesis of anisotropic peanut-like titanium oxide particles

0.2 g as-obtained monodispersed TiO_2 spherical particles were dispersed in 50 mL deionized water with sonicating 0.5 h. Then different amounts (i.e. 1 g, 2 g, 5 g) of glacial acetic acid (GAA) was added into the above solution and continue stirred for 6 h. Subsequently, the products were separated by centrifugation, washed with deionized water until the pH of the solution was nearly 7. The product of anisotropic peanut-like titanium oxide was dispersed in 30 mL deionized water.

2.3. Synthesis of anisotropic TiO_2/PANI nanocomposites

30 mL as-obtained anisotropic titanium oxide solution was mixed with 1.5 mL aniline (An), 0.3 g CTAB and 1.8 g of glacial acetic acid at ice bath. The solution was mixed completely using a magnetic stirrer for about 2 h to form a uniform suspension at ice temperature. Then, 10 mL deionized water was mixed with 0.5537 g ammonium persulfate (APS). After mixing for about 10 min at ice temperature, APS solution was added into the above titanium oxide/An solution, continuously, stirred for about 30 min. The final product was centrifuged and washed with deionized water and ethanol for several times, then dried at 50 °C.

2.4. Characterization

The morphology of the obtained particles was observed by field emission scanning electron microscopy (FESEM, JEOL JSM-6700F). Transmission electron microscopy (TEM) images were recorded with HITACHI H-2650 high-resolution transmission electron microscopes. The accelerating voltage was 200 kV in each case. For the TEM measurements, small amounts of sample in ethanol was given an ultrasonic treatment for 5 min and then dropped onto a copper grid covered by a carbon film. Powder X-ray diffraction patterns were recorded on Rigaku D-MAX 2500/PC X-ray diffractometer with CuKα irradiation ($\lambda = 1.54178$ Å) and $2\theta = 4–80°$. The Zeta potential was investigated by the size and Zeta potential analyzer (Malvern Zetasizer Nano, UK).

The ER suspensions of anisotropic TiO_2/PANI nanocomposites were obtained as following: Before the preparation of ER fluid, the as-obtained sample was further immersed in aqueous NH_3 solution for over night. Finally, the TiO_2/PANI nanocomposities for the ER fluids was obtained by filtering, washing and drying. The obtained anisotropic TiO_2/PANI nanocomposites were dried in a vacuum oven at 80 °C for 12 h. The dried anisotropic TiO_2/PANI then was dispersed into silicone oil (Tian Jin Bodi chemical limited company, Tian Jin, China; dielectric constant $\varepsilon = 2.72–2.78$, viscosity $\eta = 486.5 \pm 24.3$ mPa s, and specific density $\rho = 0.966–0.974$ g cm^{-3} at 25 °C) to form the ER fluids (20 wt% particle concentration, w/w). The ER properties of suspensions were measured by an electrorheometer (HAAKE RheoStress 6000, Thermo Scientific, Germany) with a parallel plate system (PP ER35, the gap between plates was 1.0 mm), and WYZ-020 DC high-voltage generator (voltage 0–5 kV, current 0–1 mA). The steady flow curves of shear stress–shear rate were measured by the controlled shear rate (CSR) mode within 0.05–500 s^{-1} at room temperature. Before each measurement, The suspensions were presheared for 60 s at 300 s^{-1} and then applied electric fields. The yield stress was approximately obtained with the maximum shear stress at the low shear rate region. A dielectric study was carried out by using a Novocontrol broadband dielectric spectrometer at the frequency range of 0.1–10^6 Hz (Novolcontrol Technologies GmbH & Co. KG). All experiments were performed at 25 °C.

3. Results and discussion

3.1. The morphology of monodispersed titanium oxide nanospheres

The morphology of the titanium oxide nanospheres is shown by SEM images in Fig. 1(a) and (b). It was found that the titanium oxide nanospheres synthesized by the controlled hydrolysis are nearly monodispersed. Their size distribution are uniform and their surface is smooth. The diameter of nanospheres is about 400–500 nm.

3.2. The influence of different kinds and quantities of acid on the formation of anisotropic peanut-like titanium oxide particles

As-obtained monodispersed titanium oxide nanospheres can be dissolved completely in strong acid (HCl, HNO_3, etc.). It was found that the smooth monodispersed nanospheres have disappeared after reacting with strong acid. In order to obtain the anisotropic peanut-like titanium oxide, a weak acidic acid as a solvent need to be used to etch the titanium oxide spheres, such as glacial acetic acid and critic acid etc. The SEM images of anisotropic titanium oxide obtained by using different kinds of weak acid are shown in Fig. 2: (a and b) glacial acetic acid; (c and d) oleic acid. Moreover, anisotropic titanium oxide peanut-like particles can be obtained by using weak acid. Compared the SEM images as shown in Fig. 2a–d, they have obvious differences. Although under the existence of oleic acid, anisotropic titanium oxide peanut-like particles can be formed. There, however, are much more pieces or irregular particles in Fig. 2c and d. In Fig. 2a and b, anisotropic TiO_2 can be obtained and their peanut-like shape is clear, which means that GAA is much better than the using of oleic acid.

In order to investigate the influence of acid amounts on the

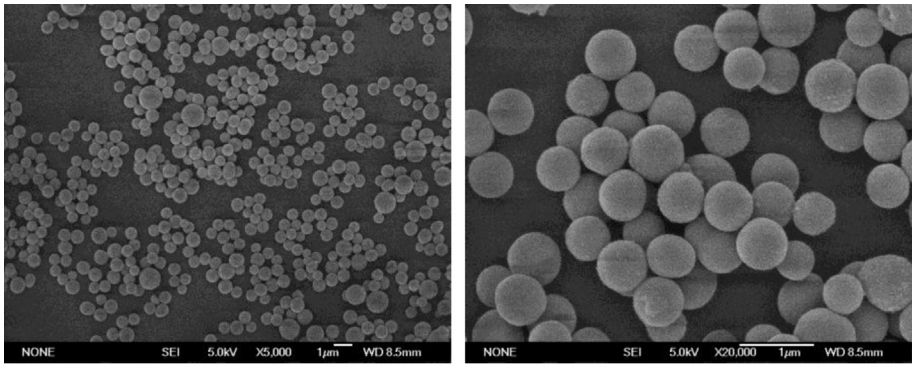

Fig. 1. The SEM image of titanium oxide under different magnification: (a) low magnification; (b) high magnification.

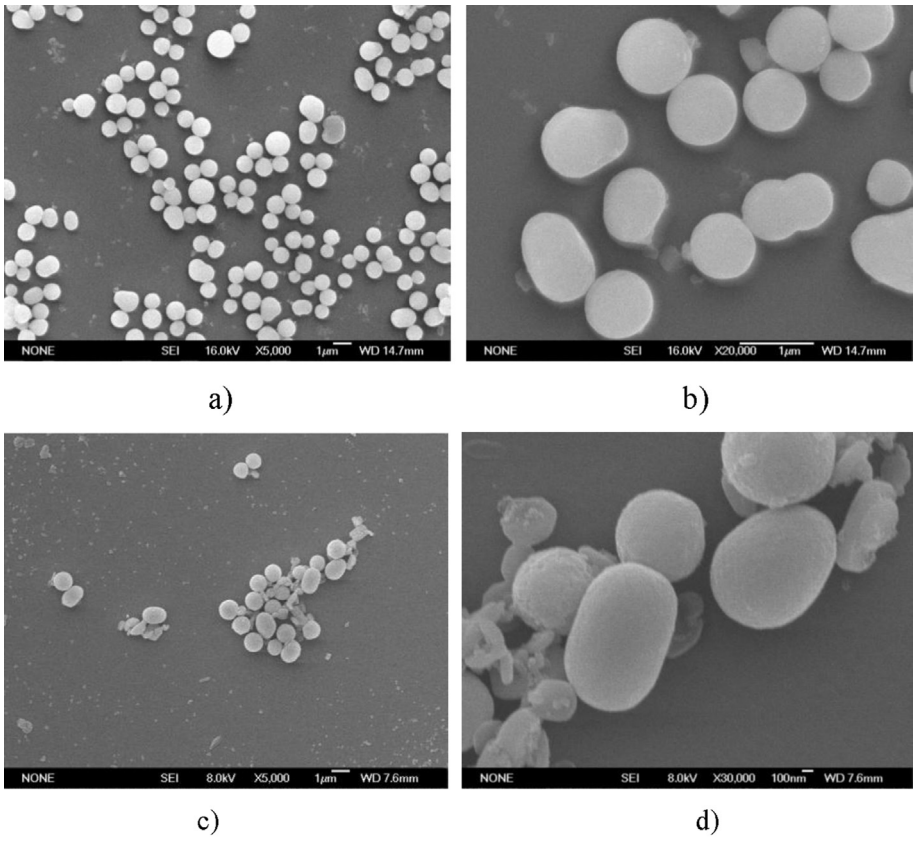

Fig. 2. The SEM images of anisotropic titanium oxide obtained by using different kinds of acid:(a and b) glacial acetic acid; (c and d) oleic acid.

morphology of anisotropic titanium oxide, different amounts of glacial acetic acid, such as 1.00 g, 2.00 g and 5.00 g etc. were used to prepare anisotropic titanium oxide, respectively. When a small amount of glacial acetic acid (i.e. 1.00 g) was added into the TiO_2 nanosphere solution, less anisotropic titanium oxide particles can be formed. With the increase in the quantity of glacial acetic acid, more anisotropic titanium oxide was obtained. If the amount of glacial acetic acid was used too much (e. g. 5 g), anisotropic titanium oxide will be continually dissolved and larger anisotropic titanium oxide containing several TiO_2 nanospheres can be formed. The result is shown in Fig. 3e and f. So it is important to control the quantity of glacial acetic acid to prepare much more anisotropic titanium oxide particles.

3.3. The effect of different dosages on the morphology of anisotropic TiO_2/PANI nanocomposites

After the formation of anisotropic peanut-like TiO_2 partilces, the *in-situ* oxidation polymerization method was used to synthsize TiO_2/PANI nanocomposite. It was found that the dosages of as-used ailine (AN) monomer also have effect on the anisotropic TiO_2/PANI core/shell structure. Fig. 4 (a, b, 1 mL AN) (c, d, 1.5 mL AN) (e, f, 2 mL AN) clearly showed the effect of AN dosages on the morphology of as-obtained TiO_2/PANI nanocomposite. Comparing Figs. 3 and 4, the surface of anisotropic TiO_2/PANI nanocompsite is much more rough than those of pure anisotropic TiO_2 in Fig. 3. It indicates that polyaniline is coated on the surface of ansiotropic TiO_2. When the

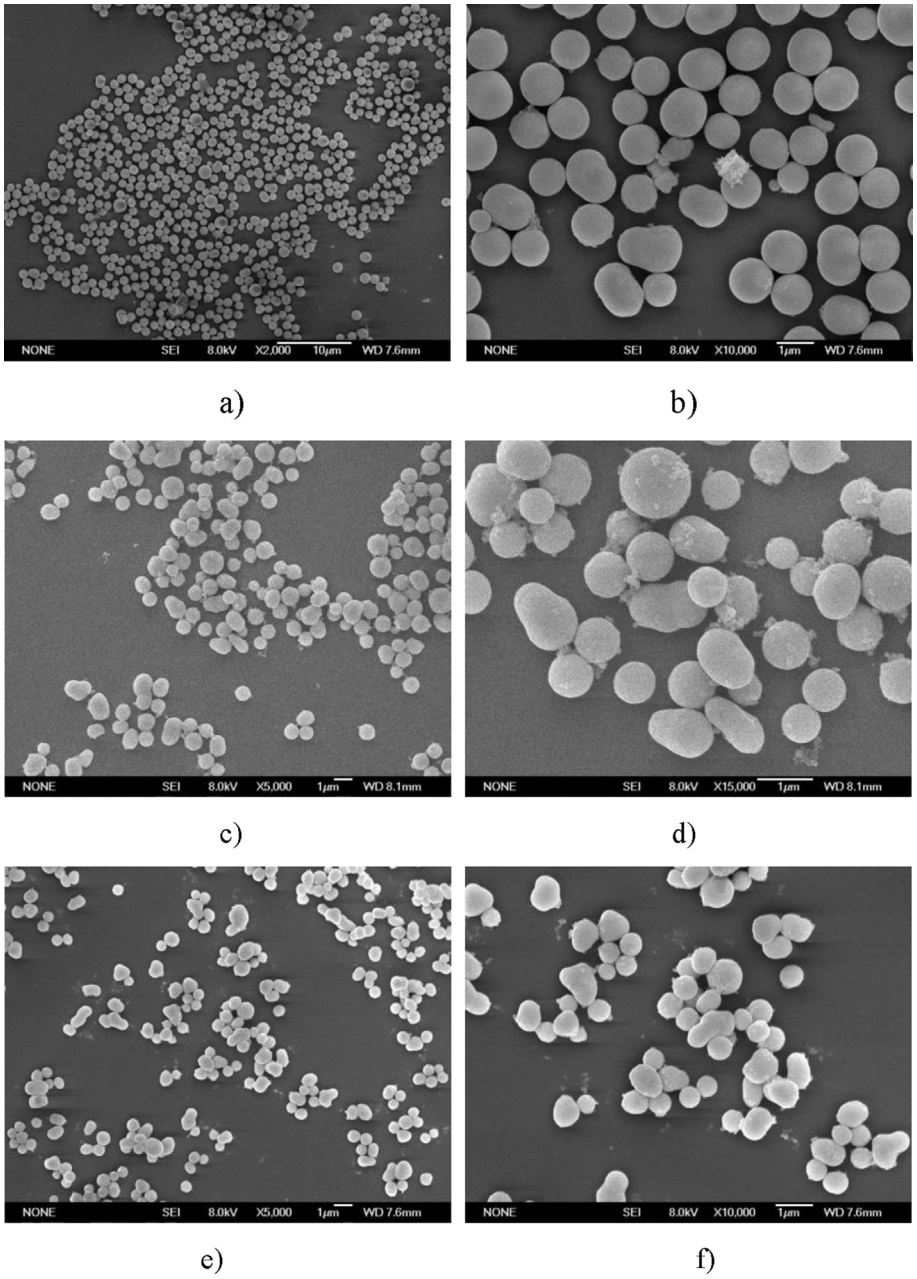

Fig. 3. The SEM picture of anisotropic titanium oxide obtained by using different quantities of glacial acetic acid: (a and b) 1.00 g; (c and d) 2.00 g; (e and f) 5.00 g.

amounts of aniline is less, it will be covered with a thin layer polyaniline on the surface of titanium dioxide, i.e. shown in Fig. 4a and b. With increasing the amounts of aniline, the thickness of polyaniline coated on the surface of titanium dioxide increases, e.g. shown in Fig. 4c and d. Furthermore, much more aniline may led to the homogenous and inhomogenous nucleation of polyaniline occurring simultaneously. Fig. 4e and f showed polyaniline has the trend to form thick coating and many irregular aggregated particles. TEM images (as shown in Fig. 4g–l) further confirm the peanut-like shape and core/shell structure of TiO_2/PANI nanocompsite.

The crystal structure of the samples was determined by XRD pattern. The obtained anisotropic TiO_2 exhibits amorphous structure (Fig. 5a). In Fig. 5a, the broad peak around 25° is shown the amorphous structure of titanium oxide. For pure PANI, several diffraction peak belonging to polyaniline appeared. Two features diffraction peaks at 20° and 25° belongs to the partly crystalline polyaniline. It is worth mentioning that the diffraction peak of TiO_2/PANI are similar to that of pure anisotropic TiO_2, which means that TiO_2/PANI nanocomposite possess the similar amorphous structure.

Above-mentioned anisotropic TiO_2/PANI composites were further studied via FT-IR analysis to investigate the chemical structures. Fig. 6 presents FTIR spectra of pure anisotropic TiO_2 particles, pure PANI particles, and anisotropic TiO_2/PANI composites. For the pure anisotropic TiO_2 sample, the broad band with a high intensity at 3400 cm^{-1} indicates the presence of hydroxyl groups (-OH) on the amorphous TiO_2 surface, which means that the amorphous TiO_2 may be descripted as $Ti(OH)_4$. The peaks observed at 400–800 cm^{-1} originate from the Ti-O vibrations. Furthermore, both O-H stretching vibrations and Ti-O band vibrations are very

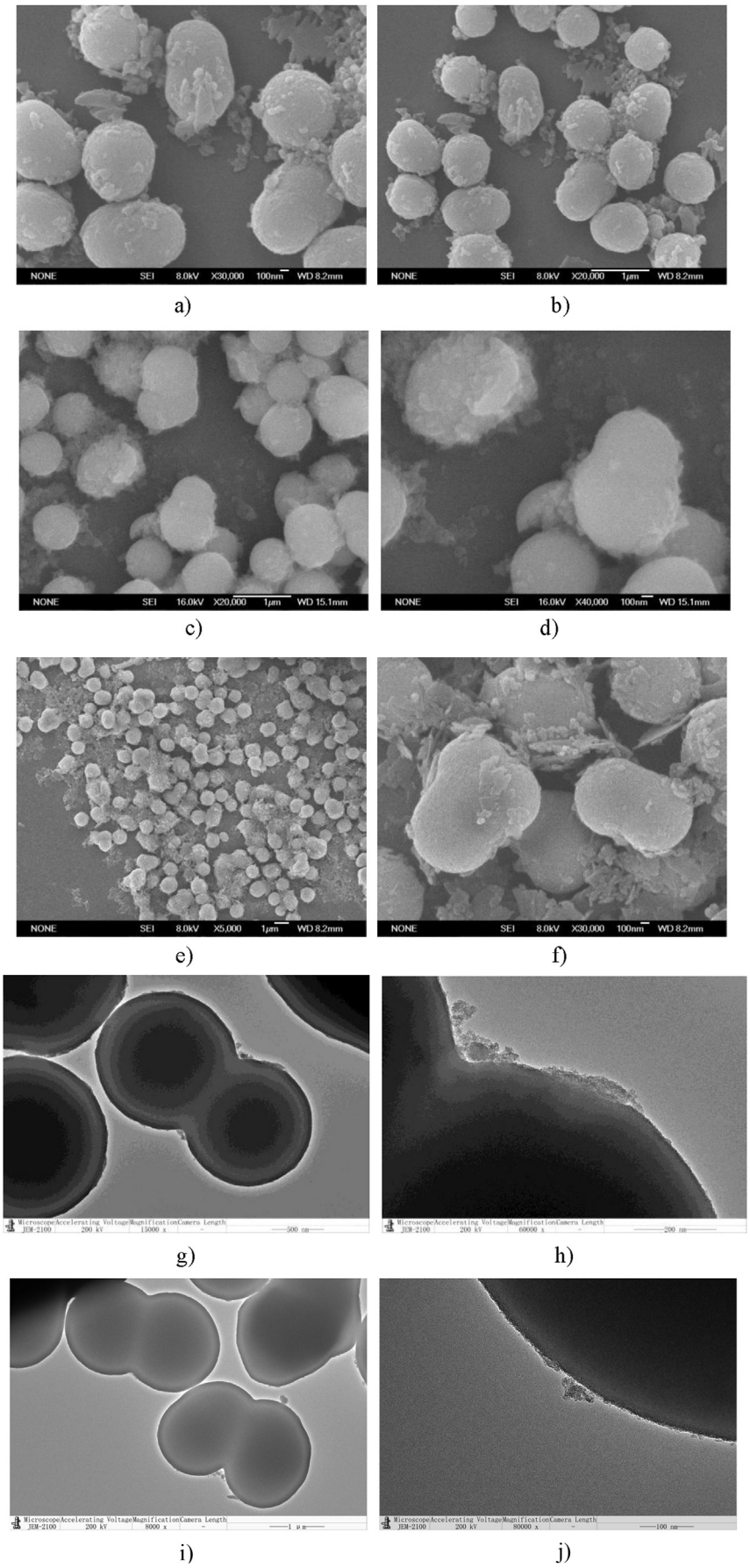

Fig. 4. SEM images of anisotropic TiO_2/PANI obtained by different dosages of aniline (a,b 1 mL AN; c, d 1.5 mL AN; e, f 2 mL AN) and TEM images of anisotropic TiO_2/PANI (g–j).

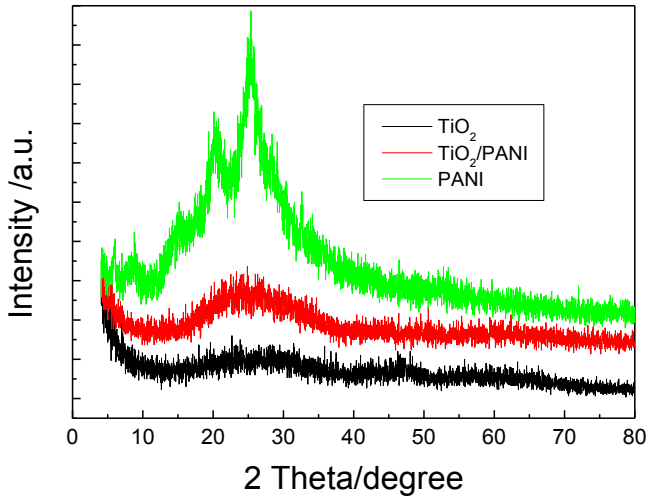

Fig. 5. XRD patterns of different samples: a) anisotropic TiO_2, b) pure PANI, c) TiO_2/PANI nanocomposite.

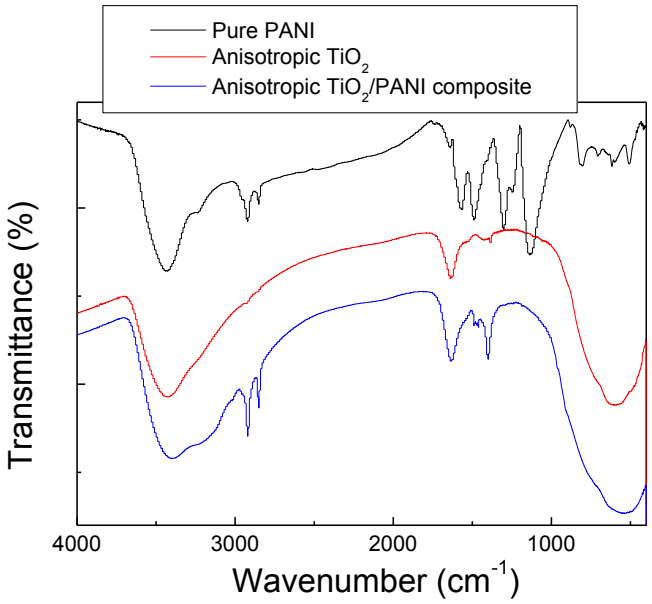

Fig. 6. FTIR spectra of pure anisotropic TiO_2 particles, pure PANI particles, and anisotropic TiO_2/PANI composites.

strong. The FTIR spectrum (Fig. 6) shows the characteristic peaks of pure PANI around 3431, 2919, 2850, 1572 (C=C stretching deformation), 1496 (vibration band of the benzenoid ring), 1289, 1139, and 799 cm^{-1}. Moreover, the vibration bands of N-H near 3431 cm^{-1} are also very strong. The C=C stretching vibration bands attributed to the quinonoid and benzenoid units appeared at 1572 and 1496 cm^{-1}, respectively. The spectrum of pure PANI exhibited two bands in the ranges 2919 and 2850 cm^{-1}, which we attribute to C-H stretching. After coated these anisotropic TiO_2 particles with PANI, the intensities of the signals around 3400 cm^{-1} for the N-H and O-H units became broader, the peaks belongs to PANI appeared consistent with the presence of PANI particles on the TiO_2/PANI composite. Especially, C-H stretching vibration of TiO2/PANI particles appeared at 2919 and 2850 cm^{-1}. The FTIR spectrum of the TiO_2/PANI particles exhibits the typical chemical characteristics of both TiO_2 and PANI particles.

The synthesis of monodispersed titanium oxide spheres can be obtained through the well-developed EG-mediated sol gel route, which was first reported by Xia's group and further modified by other groups [30–32]. It is well-known that titanium alkoxides (such as TBT, TTIP etc.) are very reactive with water, and thus white precipitates can be produced quickly even when they are in contact with moisture. However, their reactivity can be significantly reduced by using ethanol as solvent with a small amount of moisture. This reaction named as a controlled hydrolysis, which may express in the following equation:

$$Ti(OC_4H_9)_4 + 4H_2O = Ti(OH)_4 + 4C_4H_9OH \quad (1)$$

According to the results of XRD and FT-IR, anisotropic peanut-like titanium oxide particles possess amorphous structure and hydroxyl groups (-OH) existed on the amorphous TiO_2 surface. TiO_2 should be descripting as $Ti(OH)_4$. In order to obtain anisotropic TiO_2, different acids were used to react with monodispersed titanium oxide spheres. However, as-obtained monodispersed titanium oxide nanospheres can be dissolved completely in strong acid (HCl, HNO_3, etc.). For obtaining the anisotropic peanut-like titanium oxide, a weak acidic acid as a solvent need to be used to react with the titanium oxide spheres, such as glacial acetic acid and critic acid etc. Two kinds of reaction may be occurred between titanium oxide nanospheres and acid.

With strong acid, there occur dissolving reaction:

$$Ti(OH)_4 + 4H^+ = Ti^{4+} + 4H_2O \quad (2)$$

With weak acid, there may appear dehydroxylation/condensation reaction:

$$Ti(OH)_4 + Ti(OH)_4 = (OH)_3Ti{-}O{-}Ti(OH)_3 + H_2O \quad (3)$$

There may have two different kinds of etching process in this work using with strong or weak acid, which can be called completely etching and partly etching as shown in Fig. 7(a) and (b). On the one hand, when monodispersed TiO_2 spheres reacted with strong acid (such as HCl, HNO_3, etc.), dissolving reaction occurred and TiO_2 be converted into Ti^{4+}. Finally, TiO_2 spheres were completely etched and disappeared rapidly within few minutes. On the other hand, when monodispersed TiO_2 spheres reacted with weak acid (such as GAA and critic acid), dehydroxylation/condensation reaction may occur and two TiO_2 spheres combined to form an anisotropic peanut-like particle. Different anisotropic shape can be observed with the increase of etching time or acid concentration. These SEM images further confirm the condensation reaction occurred between two TiO_2 spheres.

A simple schematic diagram of experimental steps for obtaining such an ansiotropic core/shell structures is presented in Fig. 7c). It can be divided into three steps. Firstly, monodispersed TiO_2 nanospheres are synthesized through a controlled hydrolysis method. Tetrabutyl titanate (TBT) is carefully hydrolysized with a small amounts of H_2O to make uniform TiO_2 nanospheres. In the following secondary stage, weak acid is used to etch amorphous TiO_2 nanopheres and produce anisotropic peanut-like titanium oxide. Because amorphous TiO_2 be dissolved quickly in strong acid. However some weak acid also can partly dissolve amorphous TiO_2. If strictly controlling the type, dosage of weak acid, and reaction time, anisotropic TiO_2 can be obtained. Finally, polyaniline coating on the surface of anisotropic TiO_2 through a *in-situ* polymerization method was used to form a core/shell structure. To prepare composite particles with a core-shell structure, the study of zeta potential may provide an important parameter to help the formation of core/shell structure. When the potential of two components are

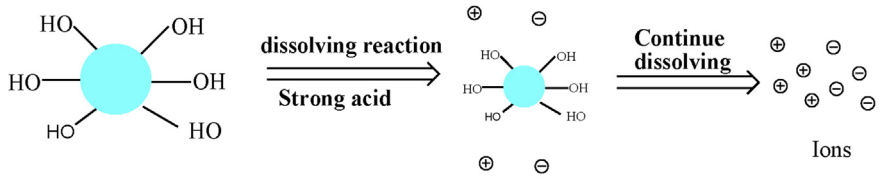

a)

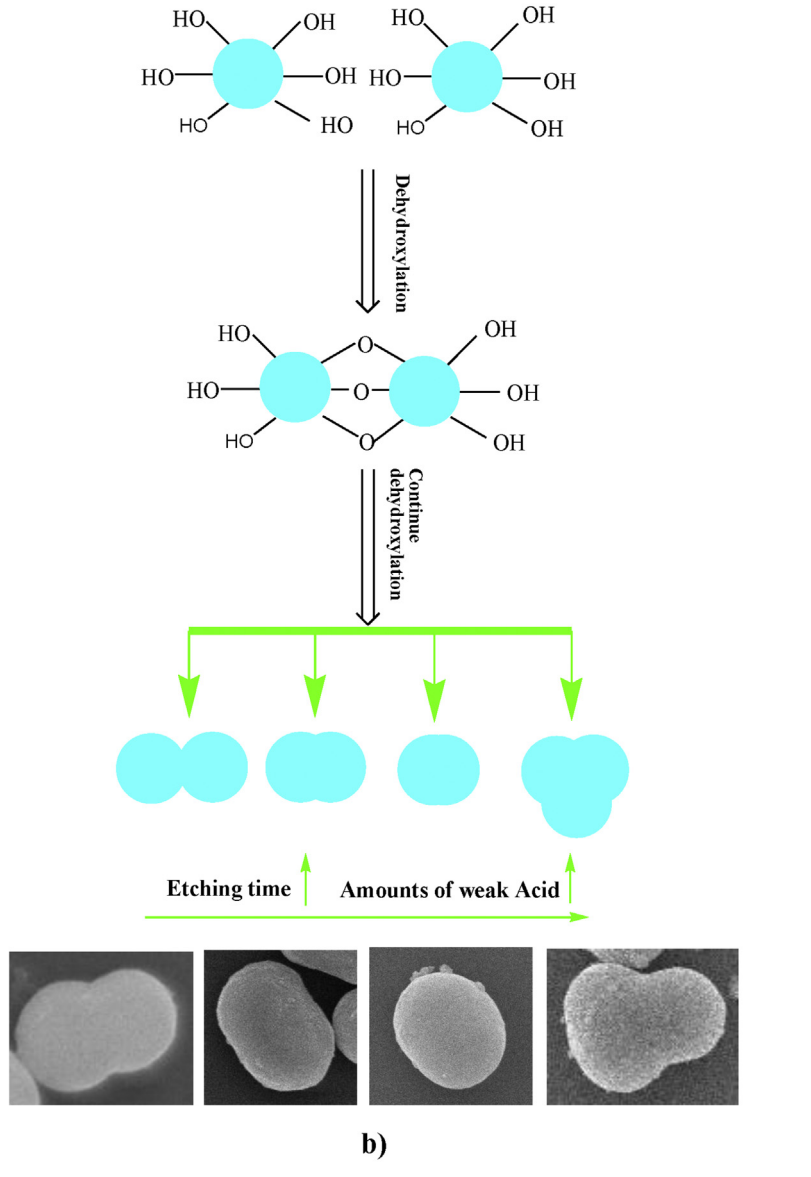

b)

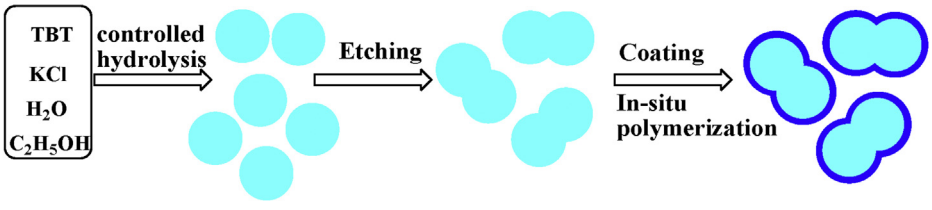

c)

Fig. 7. The schematic formation of anisotropic TiO_2 particles and anisotropic TiO_2/PANI nanocomposites: a) monodispersed TiO_2 spheres reacting with strong acid, b) monodispersed TiO_2 spheres reacting with weak acid. c) the formation of anisotropic TiO_2/PANI nanocomposites (1) Synthesis of the monodispersed titanium oxide nanospheres through controlled hydrolysis method; (2) Etching the monodisperse titanium dioxide by weak acid; (3) Synthesis of anisotropic TiO_2/PANI nanocomposites through in situ polymerization.

Table 1
Zeta potential of different samples.

Sample	Zeta potential
TiO_2	+2.65 mV
TiO_2 + CTAB	+1.56 mV
TiO_2 + GAA	+20 mV
TiO_2 + CTAB + GAA	+32.5 mV
TiO_2 + CTAB + GAA + AN	−0.447 mV

on the contrary, they can combine very well due the electrostatic interaction. The zeta potential of TiO_2 dispersion was measured as 2.65 mV as shown in Table 1. After the addition of GAA and CTAB, however, zeta potential values belonging to TiO_2 + GAA suspension were found as 20 mV and 32.5 mV for TiO_2 + CTAB + GAA suspension, which means a stable suspension for such a high zeta potential. Moreover, after the addition of aniline monomer, the zeta potential was decreased to −0.447 mV. This decrease in the absolute zeta potentials of the anisotropic TiO_2 dispersions indicated that anisotropic TiO_2 and aniline monomer have opposite potential, which is useful for the formation of TiO_2/polyaniline core-shell nanocomposite. So, anisotropic TiO_2/polyaniline core-shell structure can be formed via electrostatic interaction and may have good stability.

3.4. Electrorheological analysis

The ER suspension was prepared by dispersing the anisotropic TiO_2/PANI nanocomposites in silicone oil with a particle concentration of 20 wt%, and ER characterization was carried out using a rotational rheometer under a controlled shear rate (CSR) test. It is well-known that the external electric field has an important effect on rheological behavior of ER fluids. Its rheological property is reversible and controllable under the change of external electric field. Without external electric field, the ER fluid shows typical Newtonian fluid behavior, the shear stress of ER fluid increases linearly with the increase of shear rate. Under an external electric field, the shear stress has a larger and sudden increase when shear rate is low. It is because that, in the absence of an applied electric field, the dispersing of particles in silicone oil is random; when applying an external electric field, the particles polarized and arranged to form a chain-like structure. The ER fluid shows a typical Bingham plastic behavior under applied electric field [33–35].

The flow curves in Fig. 8 a showed the shear stresses of the ER fluid at different electric fields strength and shear rates. In the absence of external electric field, the shear stress and shear rate is approximately linear relationship. However, after applying different electric field, the shear stress of the anisotropic TiO_2/PANI nanocomposites based-ER fluid increases with the electric field strength increases from 1 to 3 kV/mm for a given shear rate. At a low shear rate, the shear stress has a larger and sudden increase, which shown a strong ER activity of anisotropic TiO_2/PANI ER suspension. Then the shear stress appears a wide plateau region as the continuing increase of shear rate. The plateau region was occurred at the low shear rate range, which reflected the competition between hydrodynamic force of particles originating from shear flow and electrostatic interaction of particles induced by electric field. Moreover, the plateau region was enlarged with the increased electric field strength. The appearance of larger plateau region indicates that the ER fluid which consisting of anisotropic TiO_2/PANI composite particles has a good rheological property. In general, the quality of electric rheological property can be calculated by a parameter so-called ER efficiency. The ER efficiency is $e = (\tau_E - \tau_0)/\tau_0$, where τ_0 is the shear stress without electric field and τ_E is the shear stress with electric field [36].

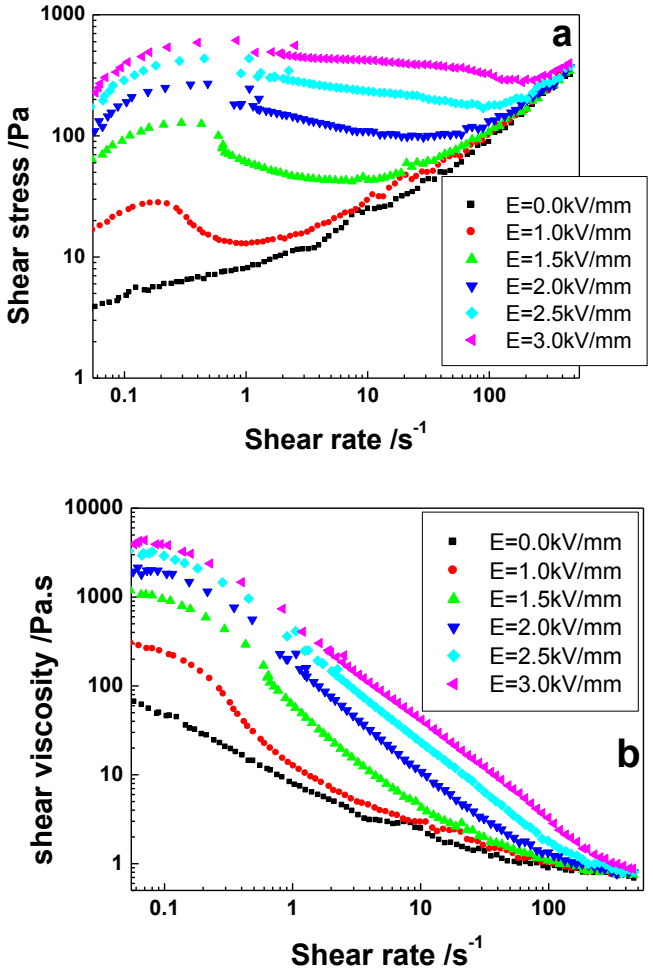

Fig. 8. Flow (a) and viscosity (b) curves of the anisotropic TiO_2/PANI ER fluid at various electric field strengths.

Figs. 8 and 9, respectively, show the steady shear flow curves measured by the controlled shear rate (CSR) mode for suspensions containing TiO_2/PANI composite with an isotropic sphere-like TiO_2 core and an anisotropic TiO_2 core under external DC electric fields. Compared to the isotropic sphere-like TiO_2/PANI composite suspension, the anisotropic TiO_2/PANI composite suspension exhibits higher shear stress and yield stress (see Figs. 8(a) and 9(a)), indicating a higher solidification activity under the same external electric field. It is also found from Fig. 8a that, after the appearance of yield stress, the shear stress of the anisotropic TiO_2/PANI composite suspension does not maintain a stable level or a plateau region as the shear rate increases and it shows a clear increase firstly, then a decline as a function of shear rate to a minimum value and then increases again. However, the shear stress of the isotropic sphere-like TiO_2/PANI suspension does not show a large decline after the appearance of yield stress (see Fig. 9a) and the plateau region of flow curves is broader than that the anisotropic TiO_2/PANI composite suspension. These different flow behaviors reveal that the two TiO_2/PANI composite suspensions possess a different ER response under the simultaneous effect of both (electrical and mechanical) fields, which will be analysis in detail with the dielectric properties. The ER efficiency (defined by $(\tau_E - \tau_0)/\tau_0$, where τ_E is the shear stress with an electric field and τ_0 is the shear stress without electric field, respectively) for the suspension of anisotropic TiO_2/PANI is much higher than that of the corresponding suspension of isotropic sphere-like TiO_2/PANI at equal

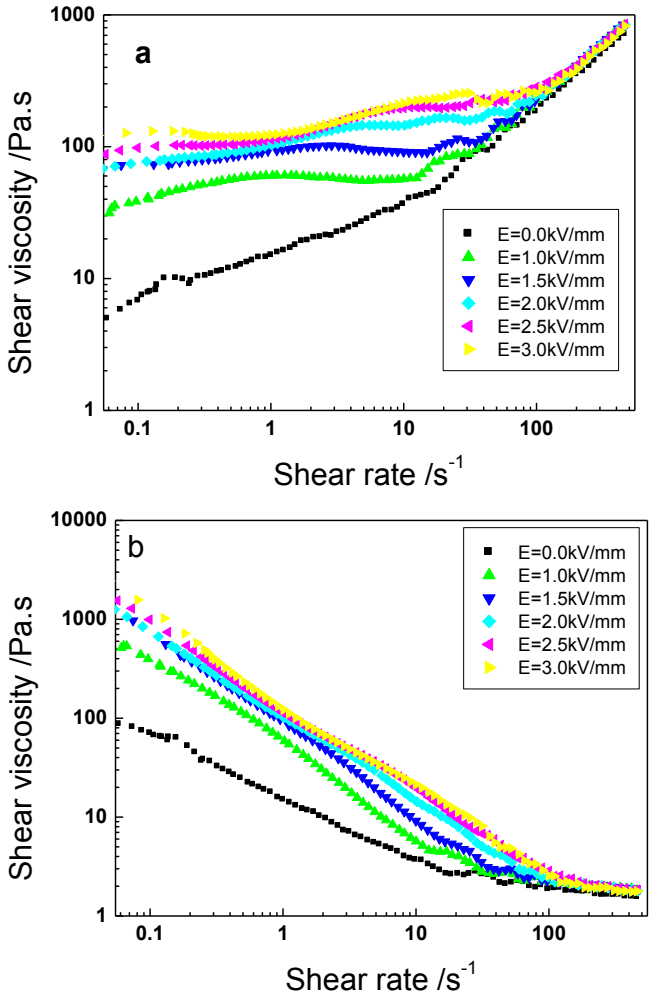

Fig. 9. Flow (a) and viscosity (b) curves of the isotropic sphere-like TiO_2/PANI ER fluid at various electric field strengths.

electric fields. The typical ER efficiency of the anisotropic TiO_2/PANI ER suspension is 74.2 (1 s^{-1}) at 3 kV/mm, which is significantly higher than that of the isotropic sphere-like TiO_2/PANI suspension (7.8 at 1 s^{-1}). Furthermore, the large polarizability of the ER particles is important to produce strong electrostatic interaction that can maintain the fibrous and column structures and thus keep the rheological properties stronger under shear flow.

Behaviors of the flow curves for the anisotropic TiO_2/PANI composite suspension is shown the increase, decrease and then increase of the shear stress with the increase of shear rate under electric fields. These phenomena are mainly associated with the change of microstructure of chains formed by polarized particles in silicone oil. It is known that the flow behavior of an ER fluid is related to the change of ER structure under the simultaneous effect of both (electrical and mechanical) fields, i.e. shearing field-induced destruction and electric field-induced reorganization of chain-like or column-like ER structure. After applying the electric field, the electrostatic forces cause the dispersed particles to form chains or columns along the electric field direction. The fibrillation of ER particles in shear flow is a breaking and re-formation process caused by the cooperation of electrostatic and hydrodynamic interactions, which are induced by an external electric and flow field. The reformation and destruction rate of particle chains depend on the competition between electrostatic and hydrodynamic forces. At low shear rate regions, the hydrodynamic interactions were small and the electrostatic interactions dominated the flow [37–39]. A breaking of these chains or columns under shear flow can led to the increase of shear stress. With the increase of shear rate, the aligned particles begin to break with shear deformation and the broken structures tend to re-form chains again. However, the rate of destruction may be faster than the rate of re-formation. Therefore, the shear stress generated decreases with increasing shear rate. When the reorganized ER structure by electric fields is not as complete as those before applying shear flow, the shear stress will decrease. The significant decrease of flow curves after the appearance of yield stress for the anisotropic TiO_2/PANI composite suspension implies that the reorganization of ER structure by electric fields is incomplete under shear flow. Furthermore, in the high shear rate region, hydrodynamic interactions dominate where fibril particle structures are fully destroyed without re-formation, and the suspension behaves like a pseudo-Newtonian fluid. So the shear stress increased again with the increase of shear rate.

The electrostatic interactions were responsible for the reorganization of ER structures and hindered the flow, while the hydrodynamic interactions tended to destroy ER structures and promoted the flow. As the shear rate increases, the hydrodynamic interactions became stronger gradually so that the destruction rate of ER structure may be faster, or still lower, or equal to the reorganization rate and thus the shear stress can decrease, or increase, or maintain with the variation of shear rate. Therefore, the different rheological curves reveal the structuring process of dispersed particles under external electric field.

Shear viscosity as a function of shear rate for the anisotropic TiO_2/PANI nanocomposites ER suspension under various different electric fields was investigated in Fig. 8b. As shown in Fig. 8b, the anisotropic TiO_2/PANI nanocomposites ER fluid showed a characteristic shear thinning phenomenon whether with an external electric field or without an external electric field. The shear thinning phenomenon means that the shear viscosity will decrease with shear rate increasing. The shear viscosity of anisotropic TiO_2/PANI nanocomposites ER fluid is clearly decreased with shear rate increasing. In addition, the shear viscosity increases with external electric field strength increasing at a same shear rate.

Fig. 10 shows the relationship of dynamic yield stress and the applied electric field strength for the anisotropic TiO_2/PANI composite suspension and isotropic sphere-like TiO_2/PANI composite suspension, respectively. This relationship can be expressed by: $\tau_y \propto E^{\alpha}$, Where τ_y is the dynamic yield stress evaluated from Figs. 8

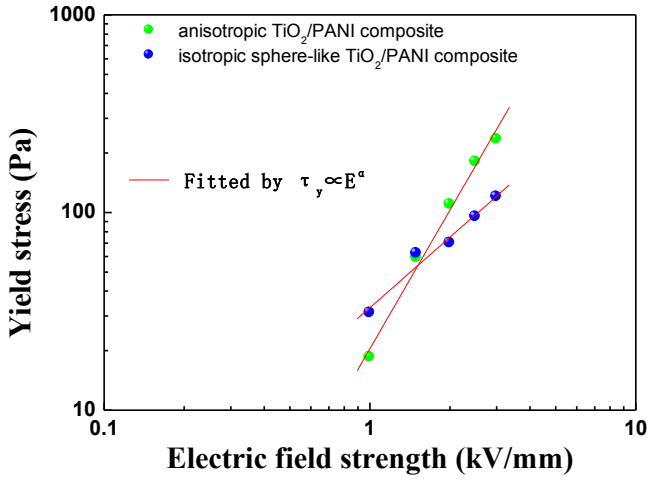

Fig. 10. Yield stress vs. electric field for the anisotropic TiO2/PANI and the isotropic sphere-like TiO_2/PANI (20 wt%)-based ER fluid.

and 9 by extrapolation [40]. The slope α of this straight line is an important parameter. When α is 2.0, this system corresponds to polarization model; and when α is 1.5, the system fits well with conductivity model. In Fig. 10, the slope was approximately 2.37 for the anisotropic TiO_2/PANI composite suspension, indicating the stronger polarization and good electro rheological properties. However, for the isotropic sphere-like TiO_2/PANI composite suspension, this value is down to 1.51, which means low ER activity comparing with that of anisotropic TiO_2/PANI composite suspension.

3.5. Dielectric analysis

Normally, the polarizability of ER materials depends on their dielectric properties. The dielectric property (expressed by $\varepsilon^* = \varepsilon'$-$i\varepsilon''$, where ε' represents the dielectric constant and ε'' represents the dielectric loss factor) can affect the ER behaviors largely. A good ER effect may require two important factors, *i.e.*, including a large $\Delta\varepsilon'$ ($\Delta\varepsilon' = \varepsilon'_{100\ Hz} - \varepsilon'_{100\ kHz}$) and a dielectric relaxation peak in ε'' within the frequency range of 10^2–10^5 Hz. Fig. 11 showed the dielectric spectra as a function of the frequency for anisotropic TiO_2/PANI based ER fluid. It is well accepted that the dielectric properties, such as dielectric constant (ε') and loss factor (ε''), are associated tightly with the interfacial polarization of ER suspensions. The larger $\Delta\varepsilon'$ and stronger ε'' can led to stronger polarized interactions among particles, which can further result a stable and stronger chain structure along the direction of electric field after the presence of external electric field. In Fig. 11, a larger dielectric loss peak belonging to the anisotropic TiO_2/PANI suspension is observed, which also mean that a relatively stronger interfacial polarizations occurred. The combination of anisotropic and core/shell structure may provide the base for the enhancement of slow polarization-interfacial polarization. Twin-like double spheres and their coating design may enrich the type and amount of conduct carrier, which are beneficial for the polarized ability. The presence of the large $\Delta\varepsilon'$ and the dielectric loss peak resulted from the dielectric mismatching between anisotropic TiO_2/PANI particles and silicone oil lead to the enhanced interfacial polarization.

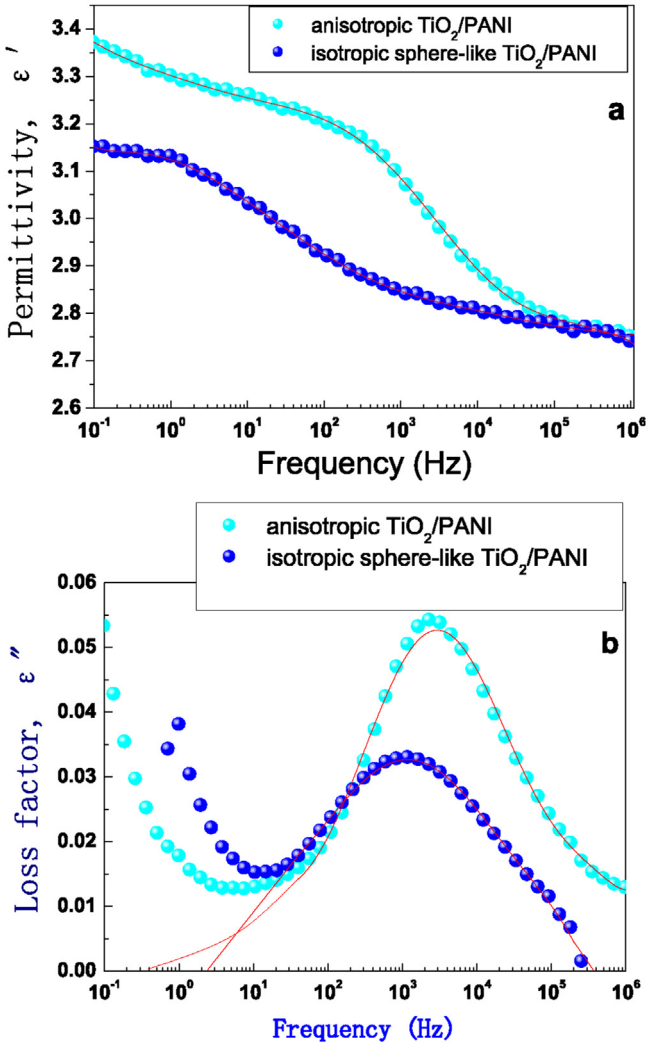

Fig. 11. Dielectric spectra of two kinds of TiO_2/PANI ER suspensions: (a) permittivity (b) loss factor. (Fitting lines are generated from the Cole–Cole equation as shown in the Formula (4)). (T = 25 °C, 20 wt%).

Concurrently, in order to investigate the ER activities for two different ER fluids (the anisotropic TiO_2/PANI composite suspension and the isotropic sphere-like TiO_2/PANI suspension) in detail, their dielectric properties were examined in Fig. 11, which may help us to explain the difference in ER effect for the two ER fluids. Fig. 11 show the dielectric spectra as a function of the frequency for 20 wt% anisotropic TiO_2/PANI and isotropic sphere-like TiO_2/PANI based ER fluids, respectively. Hence, we can see that the $\Delta\varepsilon'$ ($\Delta\varepsilon' = \varepsilon'_0 - \varepsilon'_\infty$) of normal isotropic sphere-like TiO_2/PANI 20 wt% based ER fluid is lower than that of the anisotropic TiO_2/PANI 20 wt% based ER fluid, suggesting a weak ER behavior. Moreover, it is obvious that a larger dielectric loss peak of the anisotropic TiO_2/PANI composite suspension is observed, indicating a relatively stronger interfacial/surface polarization. The presence of the large $\Delta\varepsilon'$ and the dielectric loss peak resulted from the dielectric matching between TiO_2/PANI particles and silicone oil leads to the enhanced interfacial/surface polarization.

The Cole-Cole equation, as a frequently used analysis method, has been introduced to describe the relationship between the ER effects and dielectric properties, which is used as a dielectric relaxation model to analyze the dielectric properties of ER materials [41–44]. The model is described in terms of complex dielectric constant as follows:

$$\varepsilon^* = \varepsilon\prime - \varepsilon'' = \varepsilon_\infty + \frac{\Delta\varepsilon}{1 + (i\omega\lambda)^{1-\alpha}} \quad (4)$$

Where ε_0 is the dielectric constant of an ER fluid at the low frequency limit, ε_∞ is the dielectric constant of an ER fluid at the high frequency limit, $\Delta\varepsilon = \varepsilon_0 - \varepsilon_\infty$ reflect achievable dielectric polarizability; ω is the frequency of dielectric analysis; dielectric relaxation time $\lambda = 1/2\pi f_{max}$ is the parameter resulted from maximum dielectric loss peak f_{max} at the dielectric loss curve; α is normally in the range 0–1, which (1 - α) have an influence on the broadness of the relaxation time distribution. Fig. 11 shows the dielectric spectra as a function of the frequency, and Cole–Cole fitting plot for the anisotropic TiO_2/PANI -based ER fluid analyzed by the Cole–Cole equation. The experimental data in Fig. 11 can be fitted to the well-known Cole–Cole eqn. It was well known that Δε is related to the degree of polarization of ER dispersed particles and dielectric relaxation time λ can reflect the rate of interfacial polarization [45–47].

The dielectric relaxation peak reveals the rate of polarization denoted by the relaxation time λ ($\lambda = 1/2\pi f_{max}$), where f_{max} is the local frequency of the dielectric loss peak), which is related to the stability of inter-particle interaction and the reorganization of fibril structures of ER particles. $\Delta\varepsilon'$ reveals the strength of polarization, which is related to the magnitude of inter-particle interaction

Table 2
Dielectric characteristic of the two ER suspension ($\Phi = 20$ wt%).

Sample	ε'_0	ε'_∞	$\Delta\varepsilon'$	λ(s)
Anisotropic TiO_2/PANI ER suspension	3.37	2.75	0.62	6.8×10^{-5}
Isotropic sphere-like TiO_2/PANI ER suspension	3.15	2.74	0.41	1.3×10^{-4}

induced by the external electric fields. As dielectric loss peak gets within 10^2–10^5 Hz and a larger $\Delta\varepsilon'$ is occurred, a stronger interparticle interaction or ER effect can be obtained. Considering the relaxation time, $\lambda = 1/2\pi f_{max}$, because the corresponding relaxation frequency is about 2340 Hz and 1200 Hz for anisotropic TiO_2/PANI ER suspension and isotropic sphere-like TiO_2/PANI ER suspension, so the corresponding relaxation time is 6.8×10^{-5} s and 1.3×10^{-4} s. Obviously, the above analysis on the dielectric spectra coincides with the result obtained from com-paring the shear stress.

From Table 2, we can see that the two different TiO_2/PANI suspensions all exhibit significantly dielectric relaxation peak 10^2–10^5 Hz and relatively large $\Delta\varepsilon'$. This indicates that the TiO_2/PANI particles possess large polarization strength and adequately fast polarization effect under electric fields, which is providing effective evidences for their high ER activities according to the proposed ER mechanism. When comparing two suspensions, however, it is noted that there are differences in the values of ER efficiency and $\Delta\varepsilon'$. The anisotropic TiO_2/PANI ER suspension has the larger relaxation peak and $\Delta\varepsilon'$ than those of isotropic sphere-like TiO_2/PANI ER suspension. This means that the order of strength and rate of polarization is stronger, which are agrees with the order of ER effect.

4. Conclusions

In brief, the anisotropic-like TiO_2/polyaniline core/shell structure nanoparticles has been obtained by a three-step method. Then it discussed the factors which have influence on the preparation of anisotropic-like TiO_2/polyaniline core/shell structure nanoparticles, including different kinds and different dosages of acid, the amount of aniline, and so on. The obtained anisotropic TiO_2/PANI core–shell nanoparticles exhibit a good ER behavior. The rheological test showed that the suspension consisting of anisotropic TiO_2/PANI core–shell nano-composite particles exhibits a strong ER effect. Its ER efficiency was approximately 74.2, which is really a high value. This work provides a new application for anisotropic core–shell nanocomposites as ER smart materials in the future.

Acknowledgment

Financial support from the National Natural Science Foundation of China (NSFC 51472133), the Opening Project of State Key Laboratory of Electrical Insulation and Power Equipment (Xi'an Jiaotong University, EIPE13210), the Project Sponsored by the Scientific Research Foundation for the Returned Overseas Chinese Scholars, State Education Ministry are gratefully acknowledge.

References

[1] H.J. Choi, M.S. Jhon, Electrorheology of polymers and nanocomposites, Soft Matter 5 (2009) 1562–1567.
[2] J.B. Yin, X. Xia, L.Q. Xiang, X.P. Zhao, Coaxial cable-like polyaniline@titania nanofibers: facile synthesis and low power electrorheological fluid application, J. Mater. Chem. 20 (2010) 7096–7099.
[3] W.J. Wen, X.X. Huang, S.H. Yang, K.Q. Lu, P. Sheng, The giant electrorheological effect in suspensions of nanoparticles, Nat. Mater. 2 (11) (2003) 727–730.
[4] R. Shen, X.Z. Wang, Y. Lu, D. Wang, G. Sun, Z.X. Cao, K.Q. Lu, Polar-molecule-dominated electrorheological fluids featuring high yield stresses, Adv. Mater. 21 (2009) 4631–4635.
[5] R. Tao, J.M. Sun, Three-dimensional structure of induced electrorheological solid, Phys. Rev. Lett. 67 (1991) 398–401.
[6] W.J. Wen, X.X. Huang, P. Sheng, Electrorheological fluids: structures and mechanisms, Soft Matter 4 (2008) 200–210.
[7] J.L. Jiang, Y. Tian, Y.G. Meng, Structure parameter of electrorheological fluids in shear Flow, Langmuir 27 (2011) 5814–5823.
[8] A. Lengalova, V. Pavlinek, P. Saha, J. Stejskal, T. Kitano, O. Quadrat, The effect of dielectric properties on the electrorheology of suspensions of silica particles coated with polyaniline, Phys. A 321 (2003) 411–424.
[9] M.J. Espin, A.V. Delgado, J. Plocharski, Electrorheological properties of hematite/silicone oil suspensions under DC electric fields, Langmuir 21 (11) (2005) 4896–4903.
[10] M.M. Ramos-Tejada, F.J. Arroyo, A.V. Delgado, Negative electrorheological behavior in suspensions of inorganic particles, Langmuir 26 (2010) 16833–16840.
[11] J.Y. Hong, J. Jang, Highly stable, concentrated dispersions of graphene oxide sheets and their electro-responsive characteristics, Soft Matter 8 (2012) 7348–7350.
[12] W.L. Zhang, Y.D. Liu, H.J. Choi, S.G. Kim, Electrorheology of graphene oxide, ACS Appl. Mater. Interfaces 4 (4) (2012) 2267–2272.
[13] P. Tan, W.J. Tian, X.F. Wu, J.Y. Huang, L.W. Zhou, J.P. Huang, Saturated orientational polarization of polar molecules in giant electrorheological fluids, J. Phys. Chem. B 113 (2009) 9092–9097.
[14] B.X. Wang, X.P. Zhao, Wettability of a bionic nano-papilla particle and its high electrorheological effect, Adv. Funct. Mater. 15 (2005) 1815–1820.
[15] M. Sedlacik, M. Mrlik, Z. Kozakova, V. Pavlinek, I. Kuritka, Synthesis and electrorheology of rod-like titanium oxide particles prepared via microwave-assisted molten-salt method, Colloid Polym. Sci. 291 (2011) 1105–1111.
[16] B.X. Wang, Y.C. Yin, C.J. Liu, S.S. Yu, K.Z. Chen, Synthesis of flower-like $BaTiO_3$/Fe_3O_4 hierarchical structure particles and their electrorheological and magnetic properties, Dalton Trans. 42 (2013) 10042–10055.
[17] J.B. Yin, X.P. Zhao, Enhanced electrorheological activity of mesoporous Cr-Doped TiO_2 from activated pore wall and high surface area, J. Phys. Chem. B 110 (2006) 12916–12925.
[18] M. Sedlacík, M. Mrlík, V. Pavlínek, P. Sáha, O. Quadrat, Electrorheological properties of suspensions of hollow globular titanium oxide/polypyrrole particles, Colloid Polym. Sci. 290 (2012) 41–48.
[19] Y.S. Liu, J.G. Guan, Z.D. Xiao, Z.G. Sun, H.R. Ma, Chromium doped barium titanyl oxalate nano-sandwich particles: a facile synthesis and structure enhanced electrorheological properties, Mater. Chem. Phys. 122 (2010) 73–78.
[20] J.H. Wu, G.J. Xu, Y.C. Cheng, F.H. Liu, J.J. Guo, P. Cui, The influence of high dielectric constant core on the activity of core–shell structure electrorheological fluid, J. Colloid Interface Sci. 378 (2012) 36–43.
[21] Q. Cheng, V. Pavlinek, Y. He, C. Li, P. Saha, Electrorheological characteristics of polyaniline/titanate composite nanotube suspensions, Colloid Polym. Sci. 287 (4) (2009) 435–441.
[22] Y.C. Cheng, X.H. Liu, J.J. Guo, F.H. Liu, Z.X. Li, G.J. Xu, P. Cui, Fabrication of uniform core-shell structural calcium and titanium precipitation (CTP) particles and enhanced electrorheological activities, Nanotechnology 20 (2009) 055604.
[23] B.X. Wang, C.J. Liu, Y.C. Yin, S.S. Yu, K.Z. Chen, Double template assisting synthesized core-shell structured titania/polyaniline nanocomposite and its smart electrorheological response, Compos. Sci. Technol. 86 (2013) 89–100.
[24] Y.C. Yin, C.J. Liu, B.X. Wang, S.S. Yu, K.Z. Chen, The synthesis and properties of bifunctional and intelligent Fe_3O_4@titanium oxide core/shell nanoparticles, Dalton Trans. 42 (2013) 7233–7240.
[25] J. Du, X. Lai, N. Yang, J. Zhai, D. Kisailus, F. Su, D. Wang, L. Jiang, Hierarchically ordered macro–mesoporous TiO_2–graphene composite films: improved mass transfer, reduced charge recombination, and their enhanced photocatalytic activities, ACS Nano 5 (2010) 590–596.
[26] E.J. Crossland, N. Noel, V. Sivaram, T. Leijtens, J.A. Alexander-Webber, H.J. Snaith, Mesoporous TiO_2 single crystals delivering enhanced mobility and optoelectronic device performance, Nature 495 (2013) 215–219.
[27] K. Shankar, J.I. Basham, N.K. Allam, O.K. Varghese, G.K. Mor, X. Feng, M. Paulose, J.A. Seabold, K.S. Choi, C.A. Grimes, Recent advances in the use of TiO2 nanotube and nanowire arrays for oxidative photoelectrochemistry, J. Phys. Chem. C 113 (2009) 6327–6359.
[28] T. Huang, D. Qiu, One-pot synthesis of regular rhombic titanium dioxide supracolloidal submicrometer sheet via Sol–Gel method, Langmuir 30 (2014) 35–40.
[29] F.Z. Mou, L.L. Xu, H.R. Ma, J.G. Guan, D.R. Chen, S.H. Wang, Facile preparation of magnetic γ-Fe_2O_3/TiO_2 anisotropic hollow bowls with enhanced visible-light photocatalytic activities by asymmetric shrinkage, Nanoscale 4 (15) (2012) 4650–4657.
[30] X.C. Jiang, T. Herricks, Y.N. Xia, Monodispersed spherical colloids of titania: synthesis, characterization, and crystallization, Adv. Mater. 15 (2003) 1205–1209.
[31] Y. Wang, H. Xu, X. Wang, X. Zhang, H. Jia, L. Zhang, J. Qiu, A general approach to porous crystalline TiO_2, $SrTiO_3$, and $BaTiO_3$ spheres, J. Phys. Chem. B 110 (2006) 13835–13840.
[32] S. Eiden-Assmann, J. Widoniak, G. Maret, Synthesis and characterization of porous and nonporous monodisperse colloidal TiO_2 particles, Chem. Mater. 16 (2004) 6–11.
[33] Y.D. Liu, F.F. Fang, H.J. Choi, Core–Shell structured semiconducting PMMA/

polyaniline snowman-like anisotropic microparticles and their Electrorheology, Langmuir 26 (15) (2010) 12849–12854.
[34] K. Zhang, Y.D. Liu, H.J. Choi, Carbon nanotube coated snowman-like particles and their electro-responsive characteristics, Chem. Commun. 48 (2012) 136–138.
[35] Z.B. Wang, X.F. Song, B.X. Wang, X.L. Tian, C.C. Hao, K.Z. Chen, Bionic cactus-like titanium oxide microspheres and its smart electrorheological activity, Chem. Eng. J. 256 (2014) 268–279.
[36] J.B. Yin, X.X. Wang, R.T. Chang, X.P. Zhao, Polyaniline decorated graphene sheet suspension with enhanced electrorheology, Soft Matter 8 (2012) 294–297.
[37] K. Zhang, Y.D. Liu, H.J. Choi, Carbon nanotube coated snowman-like particles and their electro-responsive characteristics, Chem. Commun. 48 (2012) 136–138.
[38] T. Plachy, M. Mrlik, Z. Kozakova, P. Suly, M. Sedlacik, V. Pavlinek, I. Kuritka, The Electrorheological behavior of suspensions based on molten-salt synthesized lithium titanate nanoparticles and their Core–Shell titanate/urea analogues, ACS Appl. Mater. Interfaces 7 (2015) 3725–3731.
[39] J.B. Yin, R.T. Chang, Y.J. Shui, X.P. Zhao, Preparation and Enhanced Electro-Responsive Characteristic of reduced graphene oxide/polypyrrole composite sheet suspensions, Soft Matter 9 (2013) 7468–7478.
[40] W.L. Zhang, Y.D. Liu, H.J. Choi, Graphene oxide coated core–shell structured polystyrene microspheres and their electrorheological characteristics under applied electric field, J. Mater. Chem. 21 (2011) 6916–6921.
[41] Y.D. Liu, B.J. Park, Y.H. Kim, H.J. Choi, Smart monodisperse polystyrene/polyaniline core–shell structured hybrid microspheres fabricated by a controlled releasing technique and their electro-responsive characteristics, J. Mater. Chem. 21 (2011) 17396–17402.
[42] J.B. Yin, R.T. Chang, Y.J. Shui, X.P. Zhao, Preparation and enhanced electro-responsive characteristic of reduced graphene oxide/polypyrrole composite sheet suspensions, Soft Matter 9 (2013) 7468–7478.
[43] J.B. Yin, X. Xia, X.X. Wang, X.P. Zhao, The electrorheological effect and dielectric properties of suspensions containing polyaniline@titania nanocable-like particles, Soft Matter 7 (2011) 10978–10986.
[44] Y.Z. Dong, J.B. Yin, J.H. Yuan, X.P. Zhao, Microwave-assisted synthesis and high-performance anhydrous electrorheological characteristic of monodisperse poly(ionic liquid) particles with different size of cation/anion parts, Polymer 97 (2016) 408–417.
[45] Y.L. Cao, H.J. Choi, W.L. Zhang, B.X. Wang, C.C. Hao, J.Q. Liu, Eco-friendly mass production of poly(p-phenylenediamine)/graphene oxide nanoplatelet composites and their electrorheological characteristics, Compos. Sci. Technol. 122 (2016) 36–41.
[46] X.Q. Ji, L. Cui, Y.H. Xu, J.Q. Liu, Non-covalent interactions for synthesis of new graphene based composites, Compos. Sci. Technol. 106 (2015) 25–31.
[47] M.X. Chen, Y.L. Shang, Y.L. Jia, J.R. Li, Novel functional materials with both electrorheological performance and luminescence property, Compos. Sci. Technol. 100 (2014) 76–82.